Phase-dependent angular distributions of photoelectrons in an infinite sequence of linearly polarized few-cycle pulses

Jingtao Zhang, Xunli Feng, and Zhizhan Xu
Laboratory for High Intensity Optics, Shanghai Institute of Optical and Fine Mechanics, Chinese Academy of Sciences, Shanghai 201800, People's Republic of China

Dong-Sheng Guo
Department of Physics, Southern University, Baton Rouge, Louisiana 70813, USA
(Received 23 July 2003; published 21 April 2004)

Above-threshold ionization of Xe atoms in an infinite sequence of linearly polarized few-cycle pluses is studied. The dependence of photoelectron angular distributions (PADs) on the carrier-envelope (CE) phase in various few-cycle pulses are obtained. Our study shows that PADs in linearly polarized few-cycle pulses vary with the CE phase. The PADs are inversion asymmetric for most CE phases and inversion symmetric for some special CE phases. The PADs are always symmetric about the polarization vector, but the maximal ionization rates vary with the CE phase. Our study also shows the jet structures in PADs arising from the inherent property of photon ionization and the variation of PADs with the number of optical cycles in a single pulse.

DOI: 10.1103/PhysRevA.69.043409 PACS number(s): 32.80.Rm, 42.50.Hz, 42.50.Vk, 42.50.Ct

I. INTRODUCTION

Recent developments in laser technology have made it possible to produce high intensity laser pulses of few optical cycles [1], which provide a powerful coherent light source with extremely high intensity in high-power laser systems. Ultrashort pulses have the advantage that a high intensity can be reached in a time span shorter than the response time in which the electron escapes from an atom, allowing much higher effective field strengths [2]. Meanwhile, for a few-cycle pulse, the temporal shape of its electric field varies dramatically with the initial phase of the carrier wave with respect to the pulse envelope. Thus, all the physical processes induced by this field depend on the value of the carrier-envelope (CE) phase, such as above-threshold ionization (ATI) of noble atoms [2,3].

The previous studies of the CE phase mainly focused on the circularly polarized pulses [2–5]. The use of circularly polarized pulses has an advantage that the amplitude of the electric field varies smoothly with time, thus the modulation on ionization due to the rapid change of electric field is avoided [6]. However, in experiments it is not easy to produce a phase-stabilized few-cycle pulse of circular polarization, which obstructs the benefits of the circular polarization [2]. Thus, the use of linearly polarized pulses is also beneficial [7–9]. In the present paper, we study the phase-dependent phenomena of ATI in linearly polarized few-cycle pulses.

Using a nonperturbative scattering theory of ATI developed by Guo, Åberg, and Crasemann [10], we studied [11] the photoionization in circularly polarized pulses and demonstrated the spacial inversion asymmetry and symmetry in photoelectron angular distributions (PADs). Even though an ultrashort pulse consists of many frequency components, a few dominant components may just mimic the short pulses. We treated the ultrashort pulse as a three-mode laser field [11]. For an n-cycle pulse, its electric field can be written as

$$\mathbf{E}(t) = \mathbf{E}_0 \sin(\omega t + \phi_0)\sin^2(\pi t/\tau) = \frac{\mathbf{E}_0}{4}[2\ \sin(\omega_1 t + \phi_0) - \sin(\omega_2 t + \phi_0) - \sin(\omega_3 t + \phi_0)], \quad (1)$$

where $\tau = 2n\pi/\omega$ is the pulse duration, ϕ_0 is the CE phase, and

$$\omega_1 = \omega, \quad \omega_2 = \omega(1 + 1/n), \quad \omega_3 = \omega(1 - 1/n). \quad (2)$$

This treatment corresponds to a series of n-cycle pulses, each of which shares a common initial phase. Variation of the common phase mimics the change of the CE phase difference of the ultrashort pulses.

In this paper we study ATI of Xe in linearly polarized few-cycle pulses and focus on the CE phase-dependent PADs in various pulses. We study the cases that the number of optical cycles is larger than one, i.e., $n > 1$. If $n = 1$, our treatment reduces to a two-mode case, which is studied by Gao *et al.* as a phase difference effect between modes [12]. We will show the dependence of PADs on the CE phase, disclose the variation of PADs with the number of cycles in a single pulse, and compare the PADs in linearly polarized pulses with those in circularly polarized pulses.

This paper is organized as follows: the quantum state of an electron in n-cycle pulses is given in Sec. II; the ionization rate and a brief analysis of inversion asymmetry are given in Sec. III; the numerical results are shown in Sec. IV; and Sec. V is our conclusions with a brief discussion.

II. A VOLKOV STATE FOR AN ELECTRON IN n-CYCLE PULSES

The quantized vector potential of the laser pulse is ($\hbar \equiv 1, c \equiv 1$)

$$\mathbf{A}(-\mathbf{k}\cdot\mathbf{r}) = \sum_{j=1}^{3} g_j(\boldsymbol{\epsilon}_j e^{i\mathbf{k}_j\cdot\mathbf{r}} a_j + \boldsymbol{\epsilon}_j^* e^{-i\mathbf{k}_j\cdot\mathbf{r}} a_j^\dagger), \tag{3}$$

where $g_j=(2V_j\omega_j)^{-1/2}$ $(j=1,2,3)$ with V_j being the normalization volume of the jth photon mode and $\boldsymbol{\epsilon}_j$ are the polarization vectors defined by

$$\boldsymbol{\epsilon}_j = [\boldsymbol{\epsilon}_x \cos(\xi/2) + i\boldsymbol{\epsilon}_y \sin(\xi/2)]e^{i\phi_j},$$

$$\boldsymbol{\epsilon}_j^* = [\boldsymbol{\epsilon}_x \cos(\xi/2) - i\boldsymbol{\epsilon}_y \sin(\xi/2)]e^{-i\phi_j}, \tag{4}$$

where ϕ_j are the phase angles of each mode relating to the CE phase as

$$\phi_1 = \pi, \quad \phi_2 = -\phi_0/n, \quad \phi_3 = \phi_0/n, \tag{5}$$

and ξ determines the degree of polarization, and $\xi=0$ corresponds to linear polarization. We have

$$\boldsymbol{\epsilon}_k\cdot\boldsymbol{\epsilon}_j = (\cos\,\xi)e^{i(\phi_k+\phi_j)}, \quad \boldsymbol{\epsilon}_k\cdot\boldsymbol{\epsilon}_j^* = e^{i(\phi_k-\phi_j)}. \tag{6}$$

The state describing a nonrelativistic electron moving in such a laser field is the quantum-field Volkov state given by [13]

$$|\Psi_\mu\rangle = V_e^{-1/2}\sum_{j_1,j_2,j_3} \exp\{i[\mathbf{P} + (u_{p1}-j_1)\mathbf{k}_1 + (u_{p2}-j_2)\mathbf{k}_2 + (u_{p3}-j_3)\mathbf{k}_3]\cdot\mathbf{r}\}\mathcal{X}_{j_1,j_2,j_3}(z)|n_1+j_1, n_2+j_2, n_3+j_3\rangle, \tag{7}$$

and the corresponding eigenenergy reads

$$\mathcal{E}_\mu = \frac{\mathbf{P}^2}{2m_e} + \sum_{i=1}^{3}(n_i + u_{pi} + \tfrac{1}{2})\omega_i, \tag{8}$$

where $\mathbf{P}$ is the momentum of the intermediate electron state moving in the field, m_e is the rest mass of electron, and V_e is the normalization volume of the electron state; $\mathbf{k}_i=\omega_i\mathbf{k}_0$, with $\mathbf{k}_0$ being the unit vector along the pulse propagation, $|n_i + j_i\rangle$ is the Fock state of the ith mode with n_i being background photons and j_i the number of transferred photons in this mode; and u_{pi} is the ponderomotive parameter of the ith mode defined as

$$u_{pi} = \frac{e^2\Lambda_i^2}{m_e\omega_i} \quad (i=1,2,3), \tag{9}$$

with $2\Lambda_i$ being the classical amplitude of the ith mode. In the expression of the Volkov state, the generalized phased Bessel function (GPB) is given by

$$\mathcal{X}_{j_1,j_2,j_3}(z) = \sum_{q_i} X_{-j_1+2q_1+q_4+q_5+q_6+q_7}(\zeta_1)X_{-j_2+2q_2+q_4-q_5+q_8+q_9}(\zeta_2) \times X_{-j_3+2q_3+q_6-q_7+q_8-q_9}(\zeta_3)X_{-q_1}(z_1)\cdots X_{-q_9}(z_9), \tag{10}$$

where the sum is performed over q_i $(i=1,2,\ldots,9)$: $-\infty<q_i<\infty$, and $X_n(z)$ is phased Bessel functions of a complex variable defined in terms of ordinary Bessel functions $J_n(r)$ by [14]

$$X_n(z) = J_n(r)e^{in\varphi} \quad \text{with} \quad z = re^{i\varphi}. \tag{11}$$

The arguments of the GPB function are defined as

$$\zeta_1 = \frac{2|e|\Lambda_1}{m_e\omega_1}\mathbf{P}\cdot\boldsymbol{\epsilon}_1, \quad \zeta_2 = \frac{2|e|\Lambda_2}{m_e\omega_2}\mathbf{P}\cdot\boldsymbol{\epsilon}_2,$$

$$\zeta_3 = \frac{2|e|\Lambda_3}{m_e\omega_3}\mathbf{P}\cdot\boldsymbol{\epsilon}_3, \quad z_1 = \frac{1}{2}u_{p1}\boldsymbol{\epsilon}_1\cdot\boldsymbol{\epsilon}_1,$$

$$z_2 = \frac{1}{2}u_{p2}\boldsymbol{\epsilon}_2\cdot\boldsymbol{\epsilon}_2, \quad z_3 = \frac{1}{2}u_{p3}\boldsymbol{\epsilon}_3\cdot\boldsymbol{\epsilon}_3,$$

$$z_4 = \frac{2e^2\Lambda_1\Lambda_2\boldsymbol{\epsilon}_1\cdot\boldsymbol{\epsilon}_2}{m_e(\omega_1+\omega_2)}, \quad z_5 = \frac{2e^2\Lambda_1\Lambda_2\boldsymbol{\epsilon}_1\cdot\boldsymbol{\epsilon}_2^*}{m_e(\omega_2-\omega_1)},$$

$$z_6 = \frac{2e^2\Lambda_1\Lambda_3\boldsymbol{\epsilon}_1\cdot\boldsymbol{\epsilon}_3}{m_e(\omega_1+\omega_3)}, \quad z_7 = \frac{2e^2\Lambda_1\Lambda_3\boldsymbol{\epsilon}_1\cdot\boldsymbol{\epsilon}_3^*}{m_e(\omega_3-\omega_1)},$$

$$z_8 = \frac{2e^2\Lambda_2\Lambda_3\boldsymbol{\epsilon}_2\cdot\boldsymbol{\epsilon}_3}{m_e(\omega_2+\omega_3)}, \quad z_9 = \frac{2e^2\Lambda_2\Lambda_3\boldsymbol{\epsilon}_2\cdot\boldsymbol{\epsilon}_3^*}{m_e(\omega_3-\omega_2)}. \tag{12}$$

Because the polarization vectors are related to the CE phase, these arguments, except ζ_1 and z_1, are CE phase dependent.

III. TRANSITION RATE

The transition matrix element is given by [10]

$$T_{fi} = \sum_{\varepsilon_\mu=\varepsilon_f}\langle\phi_f(\mathbf{r}), m_1, m_2, m_3|\Psi_\mu\rangle\langle\Psi_\mu|V|\Phi_i(\mathbf{r}), l_1, l_2, l_3\rangle, \tag{13}$$

where l_i and m_i $(i=1,2,3)$ refer to the numbers of background photons in the ith mode before and after the interaction, respectively, and V is the interaction term in the Hamiltonian

$$V = -\frac{e\mathbf{P}\cdot\mathbf{A}(-\mathbf{k}\cdot\mathbf{r})}{m_e} + \frac{e^2\mathbf{A}(-\mathbf{k}\cdot\mathbf{r})\cdot\mathbf{A}(-\mathbf{k}\cdot\mathbf{r})}{2m_e}, \tag{14}$$

$\phi_f(\mathbf{r})$ is the plane wave of the final electron, $\Phi_i(\mathbf{r})$ is the bound state of the initial electron, $\mathcal{E}_i$ is the initial energy of the system

$$\mathcal{E}_i = -E_b + (l_1+\tfrac{1}{2})\omega_1 + (l_2+\tfrac{1}{2})\omega_2 + (l_3+\tfrac{1}{2})\omega_3, \tag{15}$$

in which the positive E_b is the binding energy of the initial atomic electron.

The first overlapping factor in the transition matrix element is

$$\langle\Psi_\mu|V|\Phi_i(\mathbf{r}), l_1, l_2, l_3\rangle = \frac{\Delta\mathcal{E}}{V_e^{1/2}}\mathcal{X}_{j_1,j_2,j_3}(z)^*\Phi_i(\mathbf{P}'), \tag{16}$$

where $\mathbf{P}'=\mathbf{P}+(u_{p1}-j_1)\mathbf{k}_1+(u_{p2}-j_2)\mathbf{k}_2+(u_{p3}-j_3)\mathbf{k}_3$, and $\Phi_i(\mathbf{P}')$ is the Fourier transform of the initial wave function; $j_i=l_i-n_i$ $(i=1,2,3)$ is the number of the absorbed photons in the ith mode when the electron is excited into a Volkov state, and

$$\Delta\mathcal{E} \equiv \frac{\mathbf{P}^2}{2m_e} + E_b + \sum_{i=1}^{3} (u_{pi} - j_i)\omega_i. \tag{17}$$

The second overlapping factor can be written as

$$\langle \phi_f(\mathbf{r}), m_1, m_2, m_3 | \Psi_\mu \rangle = \frac{(2\pi)^3}{V_e} \mathcal{X}_{j_1', j_2', j_3'}(z)\, \delta(\mathbf{P}_f - \mathbf{P}''), \tag{18}$$

where $\mathbf{P}'' = \mathbf{P} - (u_{p1} - j_1')\mathbf{k}_1 - (u_{p2} - j_2')\mathbf{k}_2 - (u_{p3} - j_3')\mathbf{k}_3$, and $j_i' = m_i - n_i$ is the number of transferred photons in the ith mode when the electron leaves the laser field. Then, the overall transition matrix element is worked out to be

$$T_{fi} = V_e^{-1/2} \Phi_i(\mathbf{P}_f - q\mathbf{k}) \Delta\mathcal{E} \times \sum_{j_1, j_2, j_3} \mathcal{X}_{j_1 - q_1, j_2 - q_2, j_3 - q_3}(z_f) \mathcal{X}_{j_1, j_2, j_3}(z_f)^*, \tag{19}$$

where $q_i = l_i - m_i$ is the number of overall transferred photons in the ith mode during the interaction. The quantity

$$q = [q_1\omega_1 + q_2\omega_2 + q_3\omega_3]/\omega \tag{20}$$

determines the final kinetic energy of the photoelectron, and thus can be used to denote the order of an ATI peak. In Eq. (19), the arguments of the GPB function are reduced to

$$\zeta_{1f} = \frac{2|e|\Lambda_1}{m_e\omega_1} \mathbf{P}_f \cdot \boldsymbol{\epsilon}_1 = \frac{2|e|\Lambda_1}{m_e\omega_1} \mathbf{P}_{fx} e^{i\phi_1},$$

$$\zeta_{2f} = \frac{2|e|\Lambda_2}{m_e\omega_2} \mathbf{P}_f \cdot \boldsymbol{\epsilon}_2 = \frac{2|e|\Lambda_2}{m_e\omega_2} \mathbf{P}_{fx} e^{i\phi_2},$$

$$\zeta_{3f} = \frac{2|e|\Lambda_3}{m_e\omega_3} \mathbf{P}_f \cdot \boldsymbol{\epsilon}_3 = \frac{2|e|\Lambda_3}{m_e\omega_3} \mathbf{P}_{fx} e^{i\phi_3}, \tag{21}$$

while other arguments are kept unchanged, and $\mathbf{P}_{fx} = |\mathbf{P}_f| \sin\theta_f \cos\phi_f$. In Eqs. (19) and (21), $\mathbf{P}_f$ is the final momentum of the photoelectron, θ_f is the scattering angle, and ϕ_f is the azimuthal angle.

The transition rate for a given ATI peak is worked out to be

$$\frac{d^2W}{d\Omega_{p_f}} = \frac{(2m_e^3\omega^5)^{1/2}}{(2\pi)^2} (q - \epsilon_b)^{1/2} (q - 4u_{p1})^2 |\Phi_i(\mathbf{P}_f')|^2 \times \left| \sum_{q_i, j_i} \mathcal{X}_{j_1 - q_1, j_2 - q_2, j_3 - q_3}(z_f) \mathcal{X}_{j_1, j_2, j_3}(z_f)^* \right|^2, \tag{22}$$

where $d\Omega_{P_f} = \sin\theta_f d\theta_f d\phi_f$ is the differential solid angle of the final photoelectron, and the sum is performed over all the possible q_i and j_i ($i = 1,2,3$), satisfying the energy conservation relation, and $\mathbf{P}_f' = \mathbf{P}_f - q\mathbf{k}_1$. The emission rate of a given ATI peak is obtained by integrating over the solid angle, and the PAD denotes the emission for different azimuths at a fixed scattering angle.

It has been shown that in a linearly polarized field, electrons are mostly emitted along the laser polarization and the PADs are of fourfold azimuthal symmetry [15]. The number of emitted electrons in the azimuthal angle ϕ_f equals that in the opposite direction, say, in the angle $\phi_f + \pi$. We term this phenomenon as inversion symmetry in the present paper. When many transition channels are involved the inversion symmetry disappears [11]. It can be shown as follows: In the polarization plane defined by $\theta_f = \pi/2$, the space reflection, which means $\phi_f \to \phi_f + \pi$, results in a phase change in the GPB function as follows:

$$\mathcal{X}_{j_1, j_2, j_3}(z|_{-\mathbf{p}_f}) = (-1)^{j_1 + j_2 + j_3} \mathcal{X}_{j_1, j_2, j_3}(z|_{\mathbf{p}_f}). \tag{23}$$

Thus, the transition rate subjected to the space reflection changes to

$$\left.\frac{d^2W}{d\Omega_{p_f}}\right|_{-\mathbf{p}_f} = \frac{(2m_e^3\omega^5)^{1/2}}{(2\pi)^2} (q - \epsilon_b)^{1/2} (q - 4u_{p1})^2 |\Phi_i(\mathbf{P}_f - q\mathbf{k}_1)|^2 \left| \sum_{q_i} (-1)^{q_1 + q_2 + q_3} \sum_{j_i} \mathcal{X}_{j_1 - q_1, j_2 - q_2, j_3 - q_3}(z_f) \mathcal{X}_{j_1, j_2, j_3}(z_f)^* \right|^2. \tag{24}$$

The space reflection leads to an additional factor related to those q_i. The sum over q_i determines whether the transition rate changes or not. We identify one set of q_i satisfying Eq. (20) for a fixed q as one transition channel, thus one channel means one possible combination of the absorbed photons from different laser modes during the ionization of an electron. The phase of each channel varies with the value of q_i, thus different channels are of different phases. When several channels are involved to form an ATI peak, the interference among channels will affect the ionization rate. If each ATI peak allows only one channel, the ionization rate is the same as that in the opposite direction. But, when several transition channels are involved to form an ATI peak, the interference will cause a distinct ionization rate from that in the opposite directions. Detailed studies show that channels with $q_2 = q_3$ are indistinguishable and thus are regarded as one.

IV. PADS IN VARIOUS PULSES

With the transition-rate formula in Eq. (22), we obtain the angular distribution of the ejected electrons. We choose Xe as the sample atom in the calculation. The wave function is chosen as that of the outermost shell $5P_{3/2}$ with binding energy 12.1 eV. The linearly polarized laser pulse is of central wavelength 800 nm and peak intensity $I = 5 \times 10^{13}$ W/cm^2.

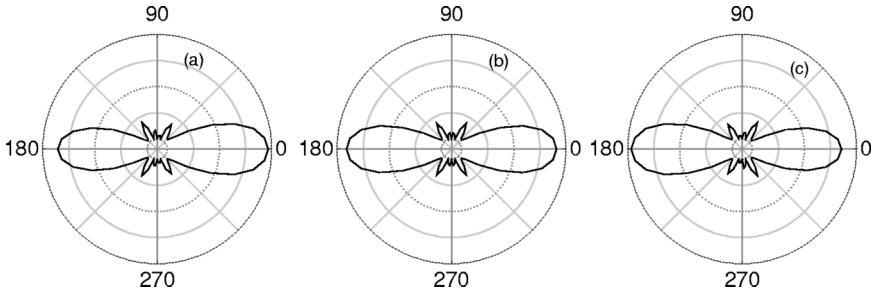

FIG. 1. The polar plots of the calculated PADs of the second ATI peak in nine-cycle pulses. The CE phase of each plot is (a) $\phi_0=0°$; (b) $\phi_0=90°$; and (c) $\phi_0=180°$. The linearly polarized laser is of central wavelength 800 nm and intensity $I=5\times10^{13}$ W/cm^2.

In what follows, we study the PADs for various few-cycle pulses. Since the ionization rate decreases rapidly with the ATI order, we just calculate PADs for low order peaks.

A. Inversion asymmetry and symmetry in PADs

Our calculations show that in long-pulse cases, where only one channel is involved to form an ATI peak, PADs exhibit the fourfold symmetry, which agrees with earlier studies for linear polarization [15]. The fourfold symmetric PADs show the little dependence on the CE phase. The ejected electrons distribute mostly along the polarization vector and thus form the main lobe of PADs. When many channels with various phases are involved to form an ATI peak, due to the interference effect among different transition channels, the inversion asymmetry appears in PADs and the fourfold symmetry reduces to a twofold symmetry in PADs. The inversion asymmetry for relatively longer pulses is slight, as shown in Fig. 1 for nine-cycle pulses; the inversion asymmetry is evident for further short pulses, and the photoelectrons are ejected out mostly in one direction determined by the CE phase, as shown in Figs. 2 and 3 for seven-cycle and five-cycle pulses, respectively. Thus, we conclude that at a fixed pulse length, the photoelectrons emit mostly in one direction determined by the CE phase. This phenomenon makes it possible to control the optimal emission of photoelectrons.

In the absence of the inversion symmetry, the PADs are still symmetric about the polarization vector. This symmetry of PADs is resulted from the symmetry of the electric field corresponding to its maximum in each single pulse. The symmetry in the case of linear polarization differs from that in the case of circular polarization [11]. In the circular polarization case, the PADs are symmetric about an axis related to CE phase, but the maximal emission rate keeps constant and has no relation with the CE phase. While in the linear polarization cases, the PADs are always symmetric about the polarization vector, but the maximal emission rate varies with the CE phase. This difference is resulted from the dependence of maximal electric-field strength on the CE phase. For circularly polarized pulses, the maximum value of the electric-field strength keeps constant for various CE phases, but its position varies with the CE phase. While for linearly polarized laser pulses, the electric field is always along the polarization vector, irrespective of what the CE phase is, but the maximal electric-field strength varies with the CE phase. As a result, the maximal ionization varies with the CE phase, but the asymmetric axis of PADs is always the polarization vector. In Fig. 4 we show the variation of the maximal ionization rate with the CE phase, in the left main lobe ($\phi_f=180°$) and in the right main lobe ($\phi_f=0°$), for five-cycle and seven-cycle pulses, respectively.

B. Fourfold symmetry in PADs

Although, generally, the inversion symmetry disappears when many ionization channels are involved, the PADs are still inversion symmetric and keep the fourfold symmetry for some special CE phases, as shown in (b) for $\phi_0=0.5\pi$ in Figs. 1–3. Paulus *et al.* [2] have supposed that, when $\phi_0=0.5\pi$, the number of photoelectrons emitted to the left side ($\phi_f=180°$) must be the same as that emitted to the right side ($\phi_f=0°$), because the electric-field distribution in the pulse envelope is symmetric when $\phi_0=0.5\pi$. Our results confirm this conjecture and show that the inversion symmetry in PADs revives for $\phi_0=0.5\pi$ and 1.5π.

In circularly polarized short pulses, the PADs for $\phi_0=0.5\pi$ are still inversion asymmetric, but the number of electrons ejected to the left direction equals that ejected to the right direction; while in the linearly polarized pulses, the PADs for $\phi_0=0.5\pi$ are inversion symmetric, thus show the fourfold symmetry. This fourfold symmetry reflects the symmetric distribution of the electric field in the pulse envelope and is only determined by the CE phase. The fourfold symmetry has no relation to the pulse length and the order of ATI peaks. The fourfold symmetric PADs also appear when $\phi_0=1.5\pi$.

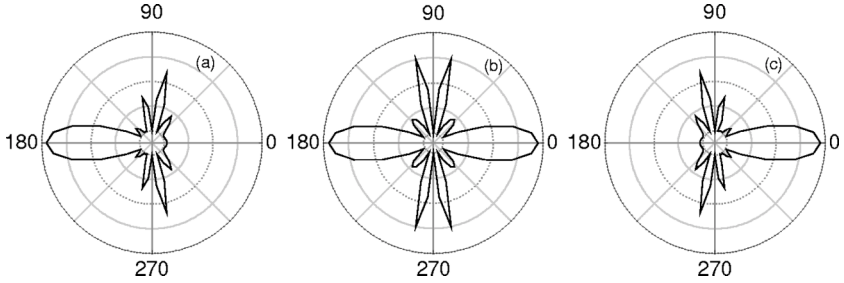

FIG. 2. Same as those in Fig. 1, but for seven-cycle pulses.

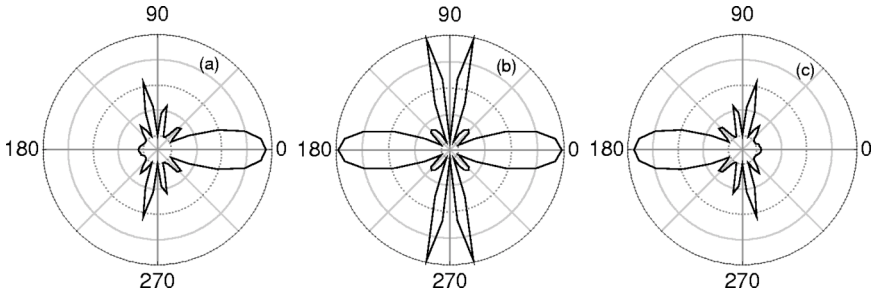

FIG. 3. Same as those in Fig. 1, but for five-cycle pulses.

C. Jet structures in PADs

Generally, the photoelectrons in a linearly polarized laser field are ejected mostly along the polarization vector, and the ejected electrons form the main lobe [16]. This kind of distribution is also confirmed by our calculations, but there are still some abnormal structures, such as those jetlike structures sticking out between the main lobes, as shown in Figs. 1–3.

The jet structures were frequently observed in experiments, such as ring structures in higher order ATI peaks [17] and the jet structures in lower order ATI peaks [16,18]. The jet structures observed in experiments are confirmed theoretically [7,19]. It has been shown that the jet structures are related to the order of ATI peaks q, the ponderomotive parameter u_p, and the binding number ϵ_b [19]. These studies are also suggestive to the present study.

The value of the GPB function increases oscillatorily with increasing the value of variables at a fixed laser intensity, thus it has many extrema. The jets in PADs are caused by the extrema of the GPB function, and the total number of jets on one side of the PADs is twice the number of the maxima in the domain of the ζ variable. Compared with the experimental observations shown in Fig. 3(b) of Ref. [16], we find two additional jets appearing in each side of the calculated PADs, as shown in Fig. 1. Because the laser field we used is of intensity higher than that for Fig. 3 of Ref. [16], the ponderomotive parameter u_p is larger, which leads to a larger ζ variable. Thus, additional jets appear.

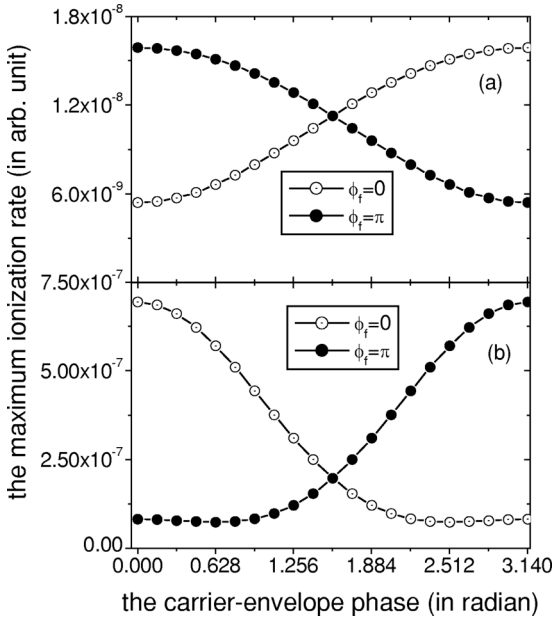

FIG. 4. Variation of the maximal ionization rate in the main lobe with the CE phase in (a) seven-cycle pulses and (b) five-cycle pulses.

D. Variation of PADs with the number of optical cycles in a single pulse

The CE phase, the number of optical cycles in a single pulse, and the final kinetic energy of a photoelectron determine the main features of PADs, and the role of the CE phase varies with the number of optical cycles in a single pulse. The CE phase shows little influence on the PADs for a long pulse, but plays an important role for ultrashort pulses.

The maximum of the main lobe varies with the CE phase and the number of optical cycles in a single pulse. The ratio of the maximal ionization in the left main lobe ($\phi_f=180°$) to that in the right main lobe ($\phi_f=0°$) varies with the CE phase, and a larger ratio is obtained in shorter pulses, as shown in Fig. 4. It is also found that for the same CE phase, the maximum ionization direction varies with the number of optical cycles in a single pulse, which is clear by comparing Fig. 2 with Fig. 3. This phenomenon provides a reference to control the ejected photoelectrons by varying the short pulse.

The jet structure of PADs is also affected by the number of optical cycles in a single pulse. When the number of optical cycles in a single pulse decreases, the jets become more prominent, as shown in Figs. 2 and 3. The enlargement of jets is also induced by the increase of the independent variable. The pulse length affects the arguments of the GPB function through the frequencies ω_i and the ponderomotive parameters u_{pi} $(i=2,3)$, and shorter pulse lengths lead to larger ζ_2 and ζ_3, thus increasing prominent jets appear.

V. CONCLUSIONS

We conclude with the following.

(1) The PADs in linearly polarized few-cycle pulses are inversion asymmetric for most of CE phases. The inversion asymmetry is resulted from the interference between transition channels. As a special case, when the CE phase is $\pi/2$ or $3\pi/2$, the PADs are inversion symmetric. This symmetry reflects the symmetric distribution of the electric field.

(2) The PADs and the maximal ionization rates along the main lobes vary with the CE phase. When the value of the CE phase is $\pi/2$ or $3\pi/2$, the ionization rates in the two poles of polarization vector equal to each other, thus the PADs show the fourfold symmetry.

(3) The PADs show the jet structure. The jet structure reflects the inherent property of photoionization.

(4) The PADs vary with the number of optical cycles in a single pulse. It is possible to optimize the PADs by varying the CE phase and the number of cycles.

In our treatment of few-cycle pulses, the electric field is no longer a single pulse, but a long sequence of *n*-cycle pulses sharing a common CE phase. If the CE phase of the *n*-cycle pulses can be stabilized in experiments, the predicted characters of PADs will be observed experimentally. Fortunately, recent developments in laser technology have made it possible to produce few-cycle pulses with a fixed CE phase [20], thus the predicted phenomena are expected to be verified experimentally in the near future.

ACKNOWLEDGMENTS

This work is supported by the Chinese National Natural Science Foundation under Grant Nos. 60178014 and 10234030, and National Key Basic Special Research Foundation under Grant No. G1999075200.

[1] M. Nisoli, S. De Silvestri, O. Svelto, R. Szipcs, K. Ferencz, Ch. Spielmann, S. Sartania, and F. Krausz, Opt. Lett. **22**, 522 (1977).

[2] G. G. Paulus, F. Grasbon, H. Walther, P. Villoresi, M. Nisoli, S. Stagira, E. Priori, and S. De Silvestri, Nature (London) **414**, 182 (2001).

[3] D. B. Milosevic, G. G. Paulus, and W. Becker, Phys. Rev. Lett. **89**, 153001 (2002).

[4] P. Dietrich, F. Krausz, and P. B. Corkum, Opt. Lett. **25**, 16 (2000).

[5] I. P. Christov, Appl. Phys. B: Lasers Opt. **70**, 459 (2000).

[6] P. Dietrich, N. H. Burnett, M. Yu, Ivanov, and P. B. Corkum, Phys. Rev. A **50**, R3585 (1994).

[7] J. P. Hansen, J. Lu, L. B. Madsen, and H. M. Nilsen, Phys. Rev. A **64**, 033418 (2001); H. M. Nilsen, L. B. Madsen, and J. P. Hansen, *ibid.* **66**, 025402 (2002).

[8] G. Duchateau and R. Gayet, Phys. Rev. A **65**, 013405 (2002); G. Duchateau, E. Cormier, H. Bachau, and R. Gayet, *ibid.* **63**, 053411 (2001).

[9] E. Mevel, P. Breger, R. Trainham, G. Petite, P. Agostini, A. Migus, J. P. Chambaret, and A. Antonetti, Phys. Rev. Lett. **70**, 406 (1993).

[10] D.-S. Guo, T. Åberg, and B. Crasemann, Phys. Rev. A **40**, 4997 (1989).

[11] Jingtao Zhang and Zhizhan Xu, Phys. Rev. A **68**, 013402 (2003).

[12] Linghui Gao, Xiaofeng Li, Panming Fu, and D.-S. Guo, Phys. Rev. A **58**, 3807 (1998).

[13] D.-S. Guo and G. W. Drake, J. Phys. A **25**, 5377 (1992).

[14] D.-S. Guo, R. R. Freeman, Lianghui Gao, Xiaofeng Li, Panming Fu, T. Edis, and A. Troha, J. Phys. B **34**, 2983 (2001).

[15] P. H. Bucksbaum, M. Bashkansky, and D. W. Schumacher, Phys. Rev. A **37**, 3615 (1988).

[16] M. J. Nandor, M. A. Walker, and L. D. Van Woerkm, J. Phys. B **31**, 4167 (1998).

[17] Baorui Yang, K. J. Schafer, B. Walker, K. C. Kulander, P. Agostini, and L. F. Dimauro, Phys. Rev. Lett. **71**, 3770 (1993).

[18] V. Schyja, T. Lang, and H. Helm, Phys. Rev. A **57**, 3692 (1998).

[19] Jingtao Zhang, Wenqi Zhang, Zhizhan Xu, Xiaofeng Li, Panming Fu, D-S Guo, and R. R. Freeman, J. Phys. B **35**, 4809 (2002).

[20] A. Baltuska, Th. Udem, M. Uiberacker, M. Henstchel, E. Goullelmakis, Ch. Gohle, R. Holzwarth, V. S. Yakovlev, A. Scrinzi, T. W. Hansch, and F. Krausz, Nature (London) **421**, 611 (2003).